Computing Danger Zones for Provably Safe Closely Spaced Parallel Approaches

Rodney Teo and Claire J. Tomlin
Stanford University, Stanford, California 94305

The use of a differential game and an optimal control theoretic approach for computing danger zones for this particular problem is new. The space outside the danger zone is deemed provably safe, implying that during blunder situations, emergency evasive maneuvers starting from outside the zone are guaranteed to be safe within limits on the maneuver severity of both the blundering and evading aircraft. In addition, these zones can be computed online in real time with knowledge of the current state. The algorithm also provides the minimum runway spacings for independent approaches and the minimum longitudinal separation between aircraft for dependent approaches. The algorithm for computing the zones has been validated with over one million simulation runs, where the adjacent aircraft performed various blunder trajectories. The validation shows that the algorithm could successfully alert and prevent collisions in 100% of the simulations ran.

Introduction

Problem

OPERATIONAL limitations exist in simultaneous approaches to airports with closely spaced parallel runways (less than 2500 ft separation). In instrument meteorological conditions (IMC), simultaneous approaches are disallowed, and the arrival rate is halved, resulting in delays and congestion. Currently, 28 airports in the United States, which include major ones such as San Francisco International Airport, are affected by this limitation. It is, therefore, beneficial to enable simultaneous approaches under such conditions; there is considerable current research focused on enabling such operations by developing airborne and ground-based systems, procedures, and associated communication links.[1−18]

In closely spaced parallel approaches (CSPA), safe operation is assured if each aircraft stays out of two zones. One contains the wake vortex of the adjacent aircraft, whereas the other is where a blunder of the adjacent aircraft could result in the separation between the two aircraft becoming less than the minimum allowed, even when an emergency evasive maneuver (EEM) is conducted. The minimum lateral separation allowed is assumed to be 500 ft, and the event in which the minimum is violated is considered a collision. As in the literature,[7] this second zone is referred to as the danger zone. The blunder could be due to a number of factors, such as pilot error, flight-control actuator failure, localizer receiver system failure, and strong gusts. A safe EEM is, thus, defined as one that does not lead to a collision. The determination and efficient computation of the danger zone are addressed in this paper.

Previous Research

In this paper, "blunderer" denotes the blundering aircraft, and "evader" denotes the aircraft that must make the EEM.

In previous research such as the segmented AILS algorithm[2,14] and the algorithm by Landry and Pritchett,[10] the "turn and straighten out" nature of the blunder trajectory is specified a priori, and variation in speed is not considered. Also, they do not explicitly consider the safety of the EEM. Because the blunder trajectory is specified, there could be other blunder trajectories that could cause a collision that are not considered. In the MITRE[3] and MIT[5] algorithms, the danger zone is obtained through Monte Carlo simulation based on a set of specific blunder trajectories. Similarly, unless the set of specific blunder trajectories is very extensive, the worst-case blunder trajectories may not be included. Besides, Monte Carlo techniques are generally computationally intensive offline.

The approach in this paper determines the danger zones by considering all blunder trajectories permitted by a model and the bounds on the control inputs, and all EEM trajectories about the nominal EEM trajectory. The latter includes the differences of the actual EEM trajectory from the nominal one. The set of blunder trajectories considered is more extensive than those in the previous algorithms. Furthermore, variations in the EEM were not considered in

Rodney Teo is a Ph.D. candidate in the Department of Aeronautics and Astronautics Engineering at Stanford University. He received his B. Eng. in mechanical engineering from the National University of Singapore in 1990 and his M. S. in aeronautics and astronautics engineering from Stanford University in 1998. He has held positions as Project Engineer (1990–1995) and Project Manager (1996–1997) on helicopter acquisition and system integration projects in the Ministry of Defense of Singapore. His research interests are in vehicle dynamics, guidance and control, and in cooperative coordination, guidance, and control of multiple vehicles. He is a Student Member of AIAA. E-mail: trodney@stanford.edu.

Claire Tomlin received her Ph.D. in electrical engineering from the University of California, Berkeley, in 1998. Since September 1998 she has been an Assistant Professor in the Department of Aeronautics and Astronautics at Stanford University, with a courtesy appointment in Electrical Engineering. She was a graduate fellow in the Division of Applied Sciences at Harvard University in 1994, and she has been a visiting researcher at NASA Ames Research Center from 1994 to 1998, at Honeywell Technology Center in 1997, and at the University of British Columbia in 1994. Claire Tomlin is a recipient of the AIAA Outstanding Teacher Award, Stanford (2001), NSF Career Award, Stanford (1999), Terman Fellowship, Stanford (1998), the Bernard Friedman Memorial Prize in Applied Mathematics, Berkeley (1998), and the Zonta Amelia Earhart Awards for Aeronautics Research (1996–1998). She was an invited participant in the National Academy of Engineering's Frontiers of Engineering Program in 2002, and she is currently a member of DARPA's Information Systems and Technology (ISAT) study group. Her research interests are in hybrid systems, air traffic control automation, flight management system analysis and design, and modeling and analysis of biological cell networks. She is a Member of AIAA. E-mail: tomlin@stanford.edu.

previous algorithms. The solution of the danger zone is obtained by applying differential game and optimal control theories. This approach, therefore, provides conditions for which an EEM can be said to be provably safe. If the evader begins the EEM outside the danger zone, it is guaranteed that a collision will not occur regardless of the sequence of control inputs chosen by both the blunderer and evader, as long as the control inputs and model parameters are within the given bounds. In addition, this approach can be implemented online.

This paper builds on work presented earlier at the Digital Avionics System Conference (DASC) in 2000[17] and at the AIAA Guidance, Navigation, and Control Conference (GNC) in 2001.[18] In the DASC paper, uncertainties in the evader's trajectory and uncertainties in the lateral speeds of both aircraft were not considered. Also, only finite duration safety guarantees were considered. In the AIAA GNC paper, the implementation and validation of the algorithm were not included.

Assumptions and Results Overview

In this approach, three specific EEMs are assumed. EEM 1 is to accelerate straight, EEM 2 is to accelerate and turn to 45 deg and then continue accelerating straight, and EEM 3 is to coast at constant speed and turn to 60 deg. In this paper, the results presented are for an evader that is performing the approach on the right of the blunderer. Thus, the turns in the EEMs 1–3 are turns to the right (away from the blunderer).

With these EEMs, the resulting danger zone will be formed by three line segments each obtained using EEMs 1–3. The zone size is a function of the aircraft speeds, relative heading, and worst-case bounds on the variation of their speeds and turn rates from nominal. The evader performing the appropriate EEM outside the corresponding boundary will be guaranteed to be safe.

These danger zones can also be used to determine the minimum safe runway separation for independent approaches (where there is no restriction on the longitudinal separation between aircraft pairs). For dependent approaches, the danger zone can be used to determine the minimum longitudinal separation (MLS) between aircraft pairs. During operations, the aircraft will operate within these minimums, and the danger zone will be computed online to alert the pilot or autopilot when to carry out the appropriate EEM in the event of blunders.

Three EEMs instead of a single EEM are used because a single EEM will not be optimal for all situations. If a single EEM without acceleration were considered, the case in which the evader is in front of a faster blunderer would not be safe. If a single EEM with acceleration were considered, the case in which the evader is to the rear of a slower blunderer would produce a very large MLS that may put the evader in the blunderer's wake.

The multiplicity of EEMs would appear to give rise to pilot training issues. However, this is not the case. For dependent approaches, the rear aircraft pilot has to be prepared to conduct only EEM 3 and the front aircraft pilot to conduct only EEM 2. (If only EEM 2 is used to form the front boundary of the danger zone, this can be done without having an impact on the MLS.) For independent approaches, EEM 2 could be used to form the whole boundary of the danger zone; this will, however, increase the size of the zone laterally, but would address the training issue. Nevertheless, the complete 3-EEM danger zone will be presented in this paper.

EEM 3 is safe for an indefinite duration only if the blunderer turns to a lesser heading or turns slower than the evader. Otherwise, EEM 3 is guaranteed to be safe only up to the end of the EEM, which is when it completes the 60-deg turn. For blunders that are due to localizer receiver system failure, pilot overcorrecting on hitting a gust, or a pilot mistaking the runway the pilot is supposed to land on, the blunderer's heading change will likely be less than that in EEM 3. Thus, EEM 3 will suffice. For a more aggressive blunder, such as when the pilot aborts the approach, but turns in the direction of the adjacent aircraft, EEM 3 will suffice if there are procedures and displays to indicate to the blundering pilot his error and that he corrects his maneuver within the duration in which EEM 3 guarantees safety. For a very aggressive blunder in which the blunderer

turns through a large angle and "pursues" the evader, such as could occur in a mechanical failure in the flight-control actuators, EEM 3 will not suffice. An adaptive algorithm used in conjunction with EEM 3 might provide protection. This adaptive algorithm could be a real-time trajectory adviser [such as the modified traffic alert and collision avoidance system (TCAS) with lateral advisories] that recommends the trajectory required to avoid a collision. The recommendation would be based on a prediction of the blunderer's trajectory.

Danger Zone Computation

As with previous research, state information of each aircraft is assumed to be available from either a local-area augmentation system (LAAS)[2] or a wide-area augmentation system (WAAS)[6] and transmitted to the other aircraft through an automatic dependent surveillance-broadcast (ADS-B)[19] datalink. The EEM is open-loop safe in that no state information of the blunderer is needed during the EEM.

Solution Overview

The approach for computing the boundary of the danger zone is as follows (Fig. 1):

1) Fix a nominal EEM as an idealized trajectory consisting of a straight segment (to account for the time lag to achieve the required bank angle and for pilot response delay) and an arc segment. The nominal EEM is chosen to be an approximation of the actual trajectory of the evader. The uncertainty bounds in forward and lateral speed, and the turn rate of the evader, are chosen so that the actual trajectory will be contained within this representation.

2) For this EEM, determine the end conditions of the computation, which are the relative position and orientation between blunderer and evader (terminal states) when a collision has just occurred.

3) Determine using optimal control techniques the worst-case control inputs required of both the blunderer and evader to drive the relative position and orientation between blunderer and evader to these end conditions, and minimize either one of the following cost functions depending on the solution sought:

a) Minimize the time to collision (game of degree).

b) Minimize the separation distance at termination (game of kind).

4) Compute (analytically, using these worst-case control inputs) the corresponding blunderer and evader state trajectory.

5) Obtain the unsafe boundary from the analytical solutions of the state propagation by repeating steps 2–5 over the space of permissible end conditions.
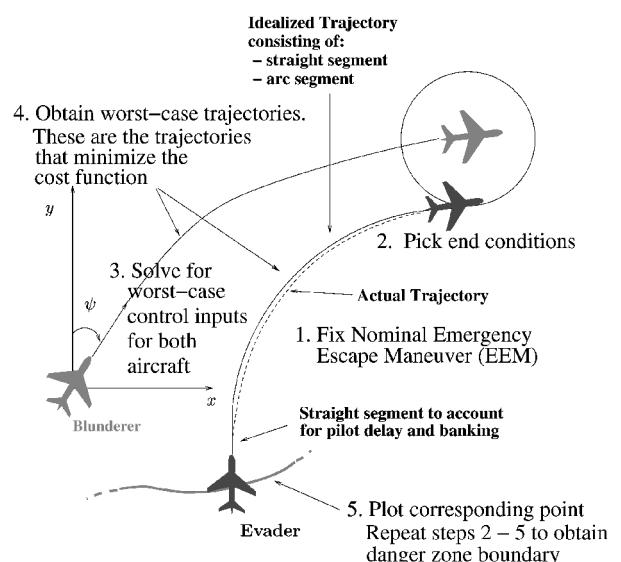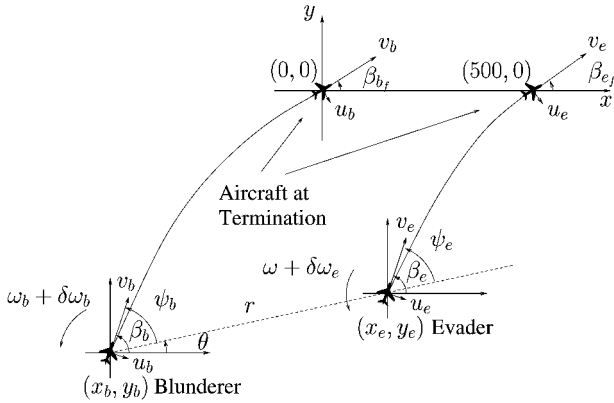

Fig. 1   Overview of approach.

y

$(0,0)$ v_b β_{b_f}

$(500,0)$ v_e β_{e_f}

u_b $\bar{x}$ u_e

Aircraft at Termination

v_e ψ_e

$\omega + \delta\omega_e$ β_e

r u_e

(x_e, y_e) Evader

$\omega_b + \delta\omega_b$ v_b ψ_b

β_b θ

u_b Blunderer

(x_b, y_b)

Fig. 2   Reference frame.

Reference Frame and Mathematical Model

In CSPA, the aircraft follow similar glide paths. They are, therefore, minimally separated in the vertical dimension. It would suffice to consider motion in the horizontal plane if the worst-case control input bounds are chosen to include three-dimensional maneuvers. The reference frame from the work of Prasad et al.[20] is chosen (Fig. 2). The worst-case control inputs of each aircraft can then be solved separately. The origin of the reference frame coincides with the blunderer position at termination and the x axis passes through the evader position at termination.

The position of the aircraft with respect to the reference frame is given by x_i and y_i, where the subscript i represents the aircraft, b for blunderer and e for evader. β_i refers to the heading of aircraft i as measured from the x axis in a counterclockwise direction.

A set of relative system coordinates is r, θ, and ψ_i. As shown in Fig. 2, they are, respectively, the distance between the two aircraft, the angle of the line joining the two aircraft as measured in a counterclockwise direction from a line parallel to the x axis, and the heading of aircraft i measured from the line joining the two aircraft in a counterclockwise direction.

Another set of relative coordinates of the evader with respect to the blunderer are $x_r = x_e - x_b$, $y_r = y_e - y_b$, and $\beta_r = \beta_e - \beta_b$. The y_r axis is in the direction of v_b.

The control inputs of each aircraft are v_i, u_i, and $\delta\omega_i$. They are, respectively, the forward speed, the lateral speed, and the variations in turn rate about the nominal turn rate of aircraft i. Finally, the subscript f attached to a state variable such as in β_{b_f} refers to the state at termination.

The equations of motion for each aircraft are given as

$$\dot{x}_i = v_i \cos(\beta_i) + u_i \sin(\beta_i)$$

$$\dot{y}_i = v_i \sin(\beta_i) - u_i \cos(\beta_i), \qquad \dot{\beta}_i = \omega_i + \delta\omega_i \quad (1)$$

The bounds on the control inputs are given as

$$v_i^{\min} \le v_i \le v_i^{\max}, \qquad -u_i^{\max} \le u_i \le u_i^{\max}$$

$$-\delta\omega_i^{\max} \le \delta\omega_i \le \delta\omega_i^{\max} \quad (2)$$

The control inputs can vary within these bounds instantaneously. Instantaneous switches will not occur in actual aircraft state dynamics. This assumption will, thus, be conservative. For the blunderer, $\omega_b = 0$ and $\delta\omega_b$ represents the variation in turn rate that is bounded equally in both the left and right directions. For the evader, ω_e is the nominal turn rate in the evasive maneuver, and $\delta\omega_e$ represents the variation in the turn rate from the nominal. Equations encapsulating the relative dynamics are given as

$$\dot{r} = v_e \cos(\psi_e) + u_e \sin(\psi_e) - v_b \cos(\psi_b) - u_b \sin(\psi_b) \quad (3)$$

$$\dot{\theta} = [v_e \sin(\psi_e) - u_e \cos(\psi_e) - v_b \sin(\psi_b) + u_b \cos(\psi_b)]/r \quad (4)$$

$$\dot{\psi}_i = \omega_i + \delta\omega_i - \dot{\theta}, \qquad \text{for} \quad i = b, e \quad (5)$$

The two different sets of states of the relative system $[(x_r, y_r, \beta_r)$ and $(r, \psi_b, \psi_e)]$ are chosen in the computation. The first set is used for presenting the danger zones with respect to the blunderer, whereas the second is used to derive the worst-case control inputs. Such a choice will result in an easier formulation for finding the worst-case control inputs.

Terminal Conditions

Recall that a collision occurs when the two aircraft are less than 500 ft apart. Thus, the terminal surface, which is the surface onto which the states are driven at the end of the game, is given as

$$T = \{r : r = 500\} \quad (6)$$

In differential game terms, the surface can be divided into the usable part (UP) and the non-UP. The boundary between these two surfaces is designated the Boundary of the UP (BUP). Only the trajectories ending on the BUP and the UP are of interest here. They are defined as

$$\text{UP} = \{T : \dot{r} < 0\}, \qquad \text{BUP} = \{T : \dot{r} = 0\} \quad (7)$$

Solving for the Worst-Case Control Inputs

Two different games with different cost functions are considered in this problem. One is with only a terminal cost, and the other is with only a running cost. In the terminal cost game (or the game of kind), the blunderer and evader aim to minimize cooperatively their separation at the end of the game, that is, when the states reach the terminal surface T. In the running cost game (or the game of degree), the blunderer and evader aim to drive the states cooperatively to the terminal surface in minimum time. Thus, the cost functions are the terminal cost game [Eq. (8a)],

$$L = 0, \qquad G = r(t_f) \quad (8a)$$

or the running cost game,

$$L = 1, \qquad G = 0 \quad (8b)$$

where L and G are the running cost and terminal cost, respectively, and t_f denotes the time at termination. The combined cost function is, thus,

$$J = \int_0^{t_f} L \, dt + G \quad (9)$$

The boundaries of the danger zone are computed from the game of kind as far as possible. In cases of EEM 3, where the blunderer turns as fast or faster than the evader, the boundary is computed from the game of degree.

When no acceleration of the evader is considered (EEM 3), the Hamiltonian is given by

$$H = p_r \dot{r} + p_{\psi b} \dot{\psi}_b + p_{\psi e} \dot{\psi}_e \quad (10)$$

From Hamilton's equations, the following equations for the costates p_r, $p_{\psi b}$, and $p_{\psi e}$ are obtained:

$$\dot{p}_r = -(p_\psi/r)\dot{\theta}, \qquad \dot{p}_\psi = p_\psi(\dot{r}/r) + p_r r\dot{\theta} \quad (11)$$

where $p_\psi = p_{\psi b} + p_{\psi e}$. The final conditions (denoted by the subscript f) on the costates are

$$p_{\psi bf} = 0, \qquad p_{\psi ef} = 0$$

$$p_{rf} = 1 \text{ (for the game of kind)}$$

$$p_{rf} = -(1/\dot{r}_f) \text{ (for the game of degree)} \quad (12)$$

Note that p_{rf} is always positive on the UP. Solving Eq. (11) with Eq. (12) gives

$$p_r = p_{rf} \cos(\theta), \qquad p_{\psi b} = -p_{rf} y_b, \qquad p_{\psi e} = p_{rf} y_e \quad (13)$$

The control inputs that minimize the cost function for both games may now be solved for. These are denoted the worst-case control inputs because any other choice of control inputs within the bounds can only improve the outcome of the game from the evader's perspective. As opposed to the min–max solution in a differential game problem,[20,21] a "min–min" problem is solved here, where the evader also tries to "assist" the blunderer in minimizing the cost function. This is used to guarantee safety even in the face of uncertainty in the model and maneuver, with respect to the evader. The worst-case control inputs are, thus, found by solving

$$\min_{\{v_b, u_b, \delta\omega_b, v_e, u_e, \delta\omega_e\}} \{H + L\} = 0 \quad (14)$$

Substituting Eqs. (10) and (13) into Eq. (14) gives

$$H = p_{rf}\{(\dot{x}_e + y_e \delta\omega_e) - (\dot{x}_b + y_b \delta\omega_b) + y_e \omega_e\} \quad (15)$$

When Eq. (1) is used and it is noted that the terms relating to each aircraft can be separated, the following provides the worst-case control inputs:

$$\max_{\{v_b, u_b, \delta\omega_b\}} \{v_b \cos(\beta_b) + u_b \sin(\beta_b) + y_b \delta\omega_b\}$$

$$\min_{\{v_e, u_e, \delta\omega_e\}} \{v_e \cos(\beta_e) + u_e \sin(\beta_e) + y_e \delta\omega_e + y_e \omega_e\} \quad (16)$$

As mentioned earlier, the worst-case control inputs can be solved for each aircraft independently of the other. This is the advantage of analyzing the problem using the chosen reference frame and the states r, ψ_b, and ψ_e.

For EEM 1 and 2, acceleration of the evader can be modeled by making v_e a state variable with $\dot{v}_e = a_e$, where a_e, a new control input, is the acceleration of the evader. The worst-case control inputs can be worked out similarly. The result turns out to be the same with $a_e = a_e^{\min}$ for all of the cases in this problem.

Obtaining Danger Zones

The worst-case trajectory for the blunderer is found by stepping backward in time from the position and heading (β_{bf}) at termination, using the equations of the trajectory with the worst-case control inputs. The worst-case trajectory ending at β_{ef} for the evader is similarly obtained.
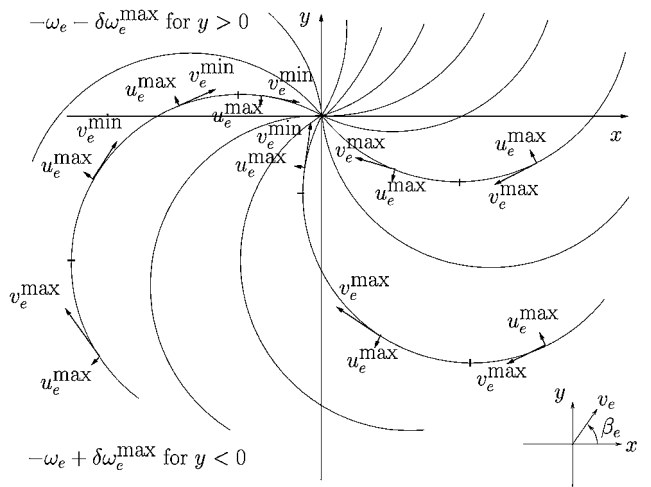
Blunderer

To be consistent with the reference frame in Fig. 2, the worst-case blunderer trajectories must end at the origin. A few sample worst-case trajectories ending at $0 \le \beta_{bf} \le 180$ are shown in Fig. 3. Those ending at $-180 \le \beta_{bf} \le 0$ are symmetric about the x axis. The arrows in Fig. 3 represent the worst-case control inputs of the blunderer as it travels along the trajectories.

Evader

For EEM 3, the worst-case evader trajectories are shown in Fig. 4. Again, to be consistent with the reference frame, the trajectories all end at $(500, 0)$, which is also on the terminal surface T. The nominal turn rate is set at a certain value ($-\omega_e$). This corresponds to a turn to the right as the evasive maneuver. Recall that, in this paper, the case of an evader performing the approach to the right of the blunderer is considered. The trajectories in Fig. 4 are, therefore, all turning right and are not symmetric about the x axis, unlike those of the blunderer. Also, note that Eq. (16) shows that the evader's worst-case control inputs are exactly the opposite of the blunderer's. Thus, the control input switches, as shown in Fig. 4, occur at the same points as the blunderer, but are of an opposite nature.
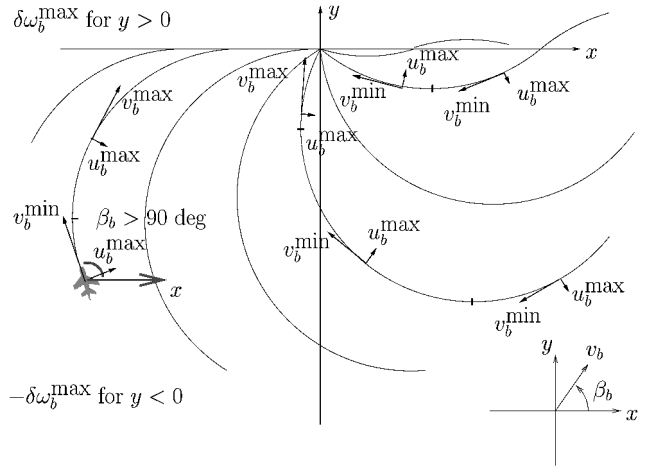
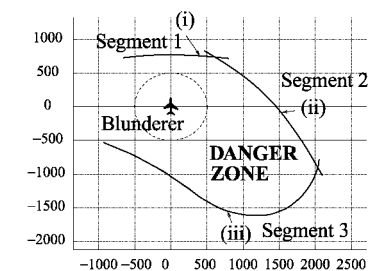**Fig. 3   Blunderer worst-case trajectories.**

Fig. 4   Evader worst-case trajectories.

The next step is to obtain the boundary of the danger zone. The boundary is generated by sweeping over all blunderer worst-case trajectories. For each blunderer worst-case trajectory, the matching evader worst-case trajectory that satisfies both the initial and terminal conditions on the relative heading β_r is found. In most cases, β_r can be solved independently of the relative position x_r, y_r. The boundary can, thus, be computed analytically without numerical integration or search. However, β_r cannot be solved independently only for a small number of cases, when the worst-case trajectory involves a turn rate switch that is a function of y_b or y_e. In this case, the solution involves a numerical search.
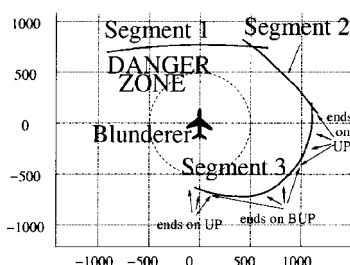
For a given relative heading, the $x - y$ space is divided into the danger and EEM safe zones. In the danger zone, there exists blunderer and evader trajectories within the bounds on the control inputs that would lead to a collision. In the EEM safe zone, all combinations of blunderer and evader trajectories within the bounds on the control inputs do not lead to a collision. Thus, provably safe evasive maneuvers can be effected outside the danger zone, starting from the given relative heading.
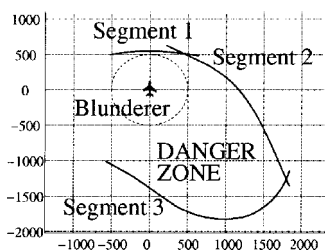
Results

This section presents the danger zones for three cases, namely, the baseline case, the sharp EEM case and the fast evader case. These three cases represent the range of cases expected in CSPA. In the baseline case, the speeds and turn rates of the blunderer and evader are similar. The parameters of the baseline case are as follows. For the blunderer, the forward and lateral speeds, and turn

a) Baseline case

b) Sharp EEM case

c) Fast evader case

Fig. 5 Danger zone boundaries (feet).

a) Evader accelerates straight

b) Evader accelerates and turns 45 deg

c) Evader turns 60 deg without acceleration

Fig. 6 Baseline case: sample worst-case trajectories (feet).

rate are $v_b = 155$–165 kn, $u_b = \pm 8$ kn, and $\omega_e = \pm 4.5$ deg/s, respectively. For the evader, the acceleration, forward and lateral speeds, turn rate, and delay are $a_e = 1$ kn/s, $v_e = 150$–160 kn, $u_e = \pm 8$ kn, $\omega_e = 4.5 \pm 0.5$ deg/s, and 3 s, respectively. The "delay" is the time in seconds between the start of the blunder and the start of the evader's acceleration and turn. This models the time required for the evader aircraft to achieve the bank angle for the turn and the time required for the engines to respond. The sharp EEM case represents situations where the evader's turn rate is faster than the bounds on the blunderer's turn rate. The parameters used are the same as the baseline case, except that $\omega_e \in [7.0, 8.0]$ deg/s. The fast evader case represents situations where the evader is faster than the blunderer. Again, the parameters used are the same as the baseline case, except that $v_b \in [145, 155]$ kn.
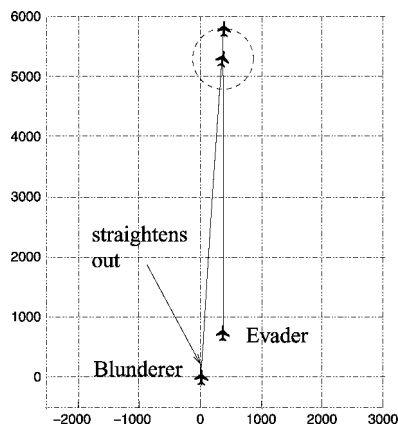
The danger zones presented are for a 0-deg relative heading. Also, only the boundary on the right of the blunderer are shown. This represents a CSPA with the evader on the right of the blunderer. Recall also that these danger zones can be computed in real time.

In all cases (Fig. 5), segments 1 and 2 are computed assuming EEM 1 and 2, respectively. In both EEMs, the evader has a minimum acceleration of 1 kn/s. Segment 3 is computed assuming EEM 3. Where acceleration of the evader is involved in the EEM, the forward speed of the evader becomes a state variable and the acceleration the control input. The forward speed will change according to the worst-case acceleration, which is the minimum acceleration in all of the cases presented.
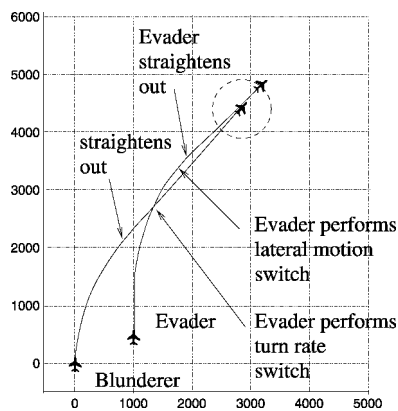
After studying these results obtained through mathematical analysis, intuitive explanations can be given.
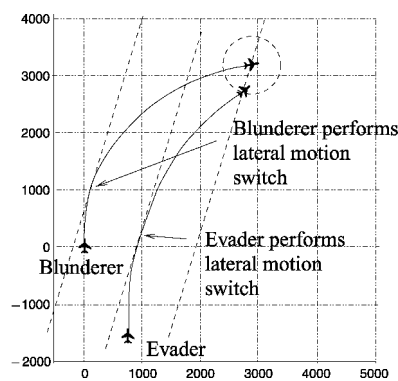
Baseline Case

The danger zone boundary for the baseline case is shown in Fig. 5a. The corresponding worst-case trajectories that generated the points i, ii, and iii on the boundary are shown in Figs. 6a, 6b, and 6c, respectively. Figure 6 shows the worst-case control input

switches, which are somewhat intuitive in hindsight. For example, in Fig. 6b, on crossing the blunderer's "future" worst-case path, the evader switches its turn rate from $-\omega_e^{\max} + \delta\omega_e$ to $-\omega_e^{\max} - \delta\omega_e$, that is, it initially turns as slowly as it can and then turns as fast as it can. The explanation would be that when the evader is to the right of the blunderer, by turning as slowly as it can, it gets itself nearer to the blunderer's path. When the evader is to the left of the blunderer, by turning as fast as it can, it gets itself back toward the blunderer's path. In addition to the turn rate switch, there is a lateral motion switch when the heading of the evader is parallel to the straight part of the blunderer's trajectory. By "slipping" leftward before the switch point and rightward after the switch point, the evader's velocity in the direction parallel to the straight part of the blunderer's trajectory is effectively reduced, thus, having a slowing down effect on the evader's motion. Because the evader terminates at the front of the blunderer, the slowing down of the evader naturally minimizes the distance between the two aircraft at termination. Though the control input switches now seem intuitive, it would have been

very difficult to predict them without the mathematical analysis. This EEM is obviously not optimal because the evader returns to the blunderer's path. The optimal heading for the evader would have been less than 45 deg. Nevertheless, to simplify the EEM procedure, a finite number of EEMs is chosen, each being suboptimal for some range of conditions.

Sharp EEM Case

The danger zone for the Sharp EEM case is shown in Fig. 5b. Note that the danger zone is smaller than that of Fig. 5a. More importantly, the solution from the game of kind appears in segment 3. This means that safety can be guaranteed indefinitely at these parts. As indicated in Fig. 5b, a part of segment 3 is generated from worst-case trajectories that end on the BUP. Recall that, in these cases, the distance between the two aircraft at termination begin to increase even if they continue to use their worst-case control inputs. This could, thus, guarantee safety indefinitely. This case shows that to have indefinite safety guarantees for a blunderer that is in front, the evader should turn more aggressively than the blunderer.

Fast Evader Case

The danger zone for the fast evader case is shown in Fig. 5c. The main difference compared to the baseline case is that the blunder zone is shifted rearward. It otherwise has the same characteristics as the baseline case.

Implementation Issues

The algorithm has been implemented both in detailed simulation, as well as for general aviation research aircraft. The additional issues addressed in the implementation are described as follows.

Communication Dropouts

It is reasonable to expect communication dropouts over a wireless link. The algorithm must be able to take into account such occurrences. There is a convenient and simple approach to handling this. The algorithm takes into account a delay before the start of the evasive maneuver; if the wireless link update rate is r hertz and if n consecutive updates are lost, the delay can be increased by n/r s to account for the dropouts. This effectively means that if the blunder starts at the beginning of the dropouts, the evasive maneuver (if required) is still guaranteed to be safe. Naturally, as the duration of consecutive dropouts increase, the danger zone will grow and could, at a certain point, lead to an encroachment over the evader.

Simplification

As it is, the danger zone boundary, for the most part, is given in the form of a series of parameterized explicit analytical expressions. (Only one case involves a bisection search algorithm.) Discontinuous switches (representing the discontinuous worst-case control switches) occur within the series. As such, a simple expression explicitly giving the boundary itself cannot be obtained. On the other hand, it is observed that the danger zone can be contained within a polygon. Because some parts of the danger zone boundary consist of relatively straight parts separated by sharp corners, about six straight lines suffice in describing the polygon with only a slight overapproximation, as shown in Fig. 7. The algorithm for checking encroachment, thus, reduces to checking that the evader is outside at least one of the sides of the polygon.

This check can be easily coded and can be performed very quickly, thus, facilitating the online implementation of the algorithm.

Sensor Inaccuracy

Sensor inaccuracy can be easily accounted for if WAAS-like characteristics are assumed. The minimum operational performance standards for WAAS[22] specify the computation of the horizontal protection level (HPL) of the differentially corrected navigation solution, which must be met at a probability of 99.99999%. This means that the true error must not exceed the protection level more than once in 10^7 s. The relative horizontal position error e between the two aircraft can, at worst, be twice the HPL with a probability of
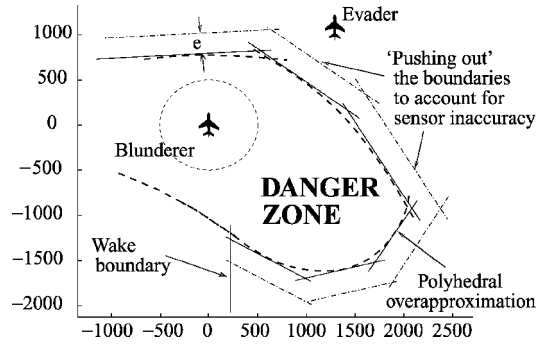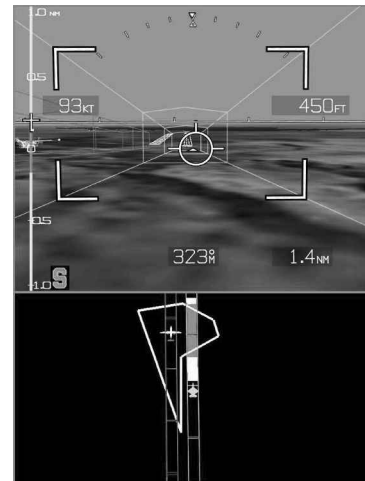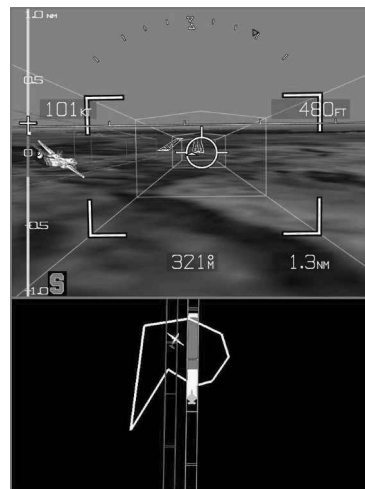

Fig. 7 Overapproximation of danger zone for online computation.

a) Normal

b) Blunder

Fig. 8 Cockpit displays (for aircraft on the right).[15]

99.99999%. The boundaries can, thus, be pushed out of the danger zone by a distance of e to account for the sensor inaccuracy. In the algorithm, this can easily be achieved by pushing out the sides of the polygon, as shown in Fig. 7.

Cockpit Display

To display the danger zones to the pilot, Jennings et al.[15] developed a cockpit display, as shown in Fig. 8, in which the algorithm was implemented in C using OpenGL and Open GVS (Quantum3D) graphics libraries on an 800-MHz Intel processor with nVidia GeForce3 graphics card. The upper half of the display is a three-dimensional perspective synthetic view, and the lower half is a map view. The danger zone is shown in the latter view as both
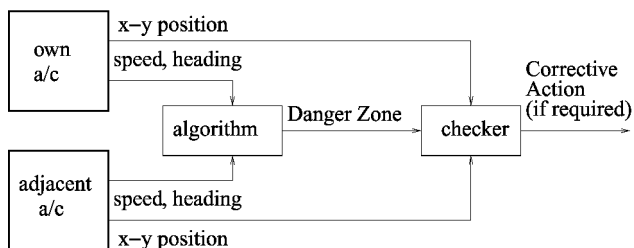
Fig. 9   Schematic showing algorithm implementation.

a polygon (as in Fig. 7) and colored strips. Only the colored strips would be displayed to the pilot. The polygon is shown here only for illustrative purposes. The colored strips indicate where the danger zone overlaps the own ship approach corridor. They are color coded to indicate the pilot response delay used in the danger zone computation. Here, the center strip, which is color coded red, represents the danger zone for a 2-s pilot response delay. The outer strips, which are color coded yellow, represent the danger zone for a 4-s pilot response delay. The pilot flying outside the yellow strip (Fig. 8a) will have 4 s to respond with a coast and turn to a 60-deg EEM when a blunder occurs (Fig. 8b) to be safe.

In sum, the schematic for the implementation of the algorithm is shown in Fig. 9. The algorithm takes speed and heading information from both aircraft and computes the danger zone polygon. With the position information from both aircraft, it then performs the check and activates the necessary EEM, if required. During the EEM, speed and heading information of the blundering aircraft will not be required.

MLS

The MLS represents the separation distance at which, under normal operating conditions, the danger zone boundary of each aircraft would not encroach on the position of the adjacent aircraft.

It is assumed that, under normal conditions, the heading of each aircraft is within ±5 deg of the nominal, so that the relative heading between a pair of aircraft is at worst ±10 deg. This assumption is based on flight simulation data on coordinated parallel runway approaches.[14] Also, it is assumed that the approach paths are rotated outward such that, under normal conditions, the lateral separation between aircraft is always greater than the runway spacing, less 200 ft. In addition, the same parameters used in the validation of the algorithm (next section) are used.

Two approach scenarios are considered. The first represents a pair of General Aviation aircraft conducting CSPA at a nominal ground speed of 100 kn, and the second represents a pair of Commercial Jet aircraft at 150 kn.

A buffer of 200 ft is added to the resulting separation and also the result is rounded off to the next one hundred feet. The buffer serves to allow variation in the longitudinal separation without triggering an EEM. The variation will be largely due to imperfect stationkeeping.

The results for a pilot response delay of 2 and 3 s are given in Table 1 for the lateral runway spacings of 750, 1700, and 2500 ft, respectively. The pilot response delays chosen are specifically significant for CSPA. Simulation studies of parallel approaches in IMC[13] revealed a mean response time of 0.71 s with a standard deviation of 0.22 s. These are significantly lower than the 5-s delay typically assumed for TCAS. However, because the final approach is a brief interval during which concentration can be maintained, short response times are possible.[16]

Because of the danger zone width, there is no MLS limitation for the 2500-ft runway case, except for the Commercial Jet scenario with a pilot response delay of 3 s. No limitation on MLS implies that independent approaches with the algorithm can be conducted. Where the MLS is nonzero, it exactly corresponds to the required separation for dependent approaches. Also, it is observed that the MLS is sensitive to pilot response delay. An increase in delay by 1 s causes the MLS to increase between 200–500 ft. The effect of poorer ADS-B reliability or lower ADS-B rate would essentially be the

Table 1   MLS vs lateral runway spacings

Airplane	Pilot response	750 ft	1700 ft	2500 ft
General Aviation	3-s delay	1900 ft	1800 ft	N/A
	2-s delay	1700 ft	1300 ft	N/A
	Automated	1300 ft	N/A	N/A
Commercial Jet	3-s delay	2400 ft	2400 ft	1900 ft
	2-s delay	2100 ft	2100 ft	N/A
	Automated	1500 ft	400 ft	N/A

same. If the ADS-B rate were 2 Hz and if the EEMs were automated, effectively eliminating the pilot response delay, the resulting MLSs would be reduced (Table 1).

Validation

The implementation of the algorithm has been validated through 1,106,091 simulations with a Piper Saratoga as blunderer and a Cessna Caravan as evader. This choice of aircraft is due to the accessibility to these aircraft for flight tests and flight-test data, yet the motivation of the algorithm is toward commercial aircraft. The simulation is performed in three dimensions, using nonlinear dynamic models whose basic control inputs are desired roll angle, lift coefficient, and thrust.

The algorithm is run online on the Cessna Caravan. It computes the danger zone boundary around the Piper Saratoga and checks the Cessna Caravan's position with respect to the boundary. On encroachment, the Cessna Caravan is made to evade according to the part of the boundary that encroaches it. The horizontal separation between the two aircraft at the closest point of approach, together with the result of each run, is recorded.

The objective of the simulation runs is to validate the algorithm with realistic aircraft models under realistic conditions involving turbulence, sensor noise, and ADS-B drop outs. Although in the simulation it is necessary to choose only a finite number of blunder trajectories, recall that the analysis considered all blunder trajectories permitted by the model and bounds on control inputs.

The validation approach is adapted from Honeywell's work.[2] With regards to the blunderer, the simulation runs consist of the following scenarios: 1) ground speeds of 100, 115, and 130 kn; 2) blunder trajectories of 60-, 30-, 15-, and 5-deg heading changes (achieved with 30-deg bank) and 10- and 5-deg constant bank; and 3) blunder flight-path angles of 1, 3, and 5 deg.

With regards to the evader, the simulation runs consist of the following scenarios: 1) ground speeds of 100, 115, and 130 kn; 2) down range of −3000 to 3000 ft at 200-ft intervals; 3) altitude of −1000 to 1000 ft at 500-ft intervals; and 4) pilot response delays of 1, 2, and 3 s.

Other variations include: 1) runway spacings of 750, 1700, and 2500 ft; 2) wind conditions that are either calm ($\sigma = 2$ ft/s) or turbulent ($\sigma = 6$ ft/s), in which σ refers to standard deviation; and 3) ADS-B reliability of 50, 70, and 90%.

The runs are made only if the evader is initially outside the danger zone. ADS-B is assumed to operate at 1 Hz. The position and velocity measurement errors were simulated by a normally distributed random number generator with standard deviations of 6.5 ft and 1 ft/s, respectively.

The mathematical model used for the aircraft is a point mass nonlinear dynamic model adapted from one developed for a NASA Air Traffic Control simulation.[23] The model is more realistic than the one used in the analysis. To obtain the speed and turn rate bounds required by the algorithm, simulations using this model were conducted under the simulated turbulent wind condition. From the resulting trajectories, the longitudinal and lateral speed variations were estimated to be ±5 kn. The maximum turn rate of the blunderer is estimated to be 6.5 deg/s. This corresponds to the turn rate achieved at a bank angle of 30 deg. For the EEMs involving a turn, the evader is assumed to bank to a maximum of 45 deg. The simulations show that these trajectories can be described by the kinematic model in Eq. (1) by a delay of 2.5 s, followed by a turn rate of 9.0 ± 0.5 deg/s.

Table 2   Outcome results

Outcome category	Alert necessary?	Alert issued?	Collision occurred?	750 ft, %	1700 ft, %	2500 ft, %
CR	No	No	No	70.1	51.2	48.5
Correct detection (CD)	Yes	Yes	No	0.4	11.0	16.0
FA	No	Yes	No	29.6	37.1	35.5
Missed detection (MD)	Yes	No	Yes	0	0	0
Induced collision (IC)	No	Yes	Yes	0	0	0
Late alert (LA)	Yes	Yes	Yes	0	0	0

Table 3   HSCPA bin/distance equivalency results from Fig. 10

Bin	distance, ft
0	<501
1	501–750
2	751–1000
3	1001–1250
4	1251–1500
5	1501–1750
6	1751–2000
7	2001–2250
8	2251–2500
9	2501–2750
A	2751–3000
B	3001–3250
C	>3250

Table 4   Metrics

Alert	Formula	750 ft, %	1700 ft, %	2500 ft, %
SA	$\dfrac{CD + FA}{CD + FA + MD + IC + LA}$	100	100	100
UA	$\dfrac{IC + FA}{CD + FA + MD + IC + LA}$	98.78	77.14	69.02
CGA	$\dfrac{IC + LA}{CD + FA + IC + LA}$	0	0	0

Fig. 10   Validation results.

are as expected because the EEM worst-case turn rate is faster than the blunderer maximum allowed turn rate. The UA metric results appear to be high. However, these alerts should be considered necessary because they are raised by blunders that have the potential to cause a collision, should their trajectories be modified midcourse. The blunders that were correctly rejected (CR) are those that did not have the potential as yet to cause a collision. It is more important to ensure that false alarms (FAs) do not occur during normal aircraft approaches with normal flight technical error (FTE). Such approaches could have been used in the validation. However, because it is evident that the algorithm will never raise an alert if the aircraft maintain the MLS, which is computed based on normal FTE, the validation was primarily focused on approaches with blunders.

The algorithm has been successfully demonstrated to work according to expectations and is able to guarantee safety as long as the blunder trajectories are captured by the model and are within the bounds on the control inputs assumed.

Conclusions

A differential game and optimal control theoretic approach for computing the danger zones for CSPA has been presented. This is the first time this approach has been applied to this particular problem. Compared to previous algorithms, this enables a more extensive range of blunder trajectories and variations in the evader emergency evasive maneuver to be considered. This approach guarantees that safe emergency evasive maneuvers can be conducted if effected outside the danger zone and if the maneuver severity of both the blunderer and evader are within the bounds assumed in computing the danger zone. In addition, this algorithm can be implemented online in real time.

The danger zone computation results can also be used to obtain the minimum runway spacing required for safe independent approaches with the algorithm running as the blunder alerting system. For dependent approaches, the results can be used to obtain the safe minimum longitudinal separation required, also with the algorithm running as the blunder alerting system. As long as the aircraft operate within the FTE used to compute the danger zones, no FAs would be raised. Further analysis shows that reduction in the MLS can be achieved with higher ADS-B rates or by automating the EEM.

The implementation issues, including a cockpit display, are addressed, and the algorithm has been validated with over one million simulation runs where the adjacent aircraft performed various blunder trajectories. The validation shows that the algorithm could successfully alert and prevent collisions in 100% of the simulations ran.
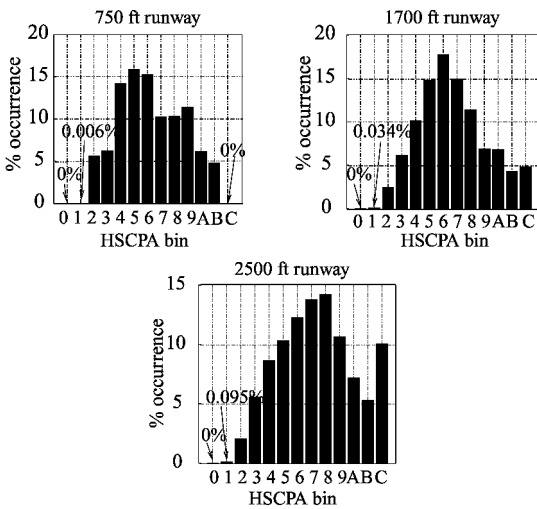
Each run consists of two subruns: one without the algorithm running and the other with the algorithm running. The result of each run is categorized according to Table 2. The simulation and algorithm are coded in C using Microsoft Visual C++ version 6.0 and are run on a Dell Pentium 3 personal computer.

Histograms of the horizontal separation at the closest point of approach (HSCPA) for the three runway spacings are shown in Fig. 10. (See also Table 3.) As expected, the HSCPA is always greater than the 500-ft minimum. Further numerical results are given in Table 2. This validates the algorithm against the chosen set of blunder trajectories and shows that it works for all of the runway spacings chosen.

As presented in the Honeywell approach (see Refs. 2 and 24), three metrics are used to evaluate the validation results. They are the probabilities of successful alert (SA), unnecessary alert (UA), and collision given an alert (CGA). The results and the corresponding formula are given in Table 4. The SA and CGA metric results

As part of future work, the online computation of the algorithm will be demonstrated in a flight experiment involving 10-ft wingspan uncrewed aircraft, and the cockpit display of the danger zone will be evaluated through piloted simulations.[15]

References

[1]Haissig, C., Corwin, B., and Jackson, M., "Designing an Airborne Alerting System for Closely Spaced Parallel Approaches," *Proceedings of the AIAA Guidance, Navigation, and Control Conference*, AIAA, Reston, VA, 1999.

[2]Jackson, M., Samanant, P., and Haissig, C., "Analysis of Airborne Alerting Algorithms for Closely Spaced Parallel Approaches," *Air Traffic Control Quarterly*, Vol. 9, No. 4, 2001, pp. 359–375.

[3]Hammer, J., "Study of the Geometry of a Dependent Approach Procedure to Closely Spaced Parallel Runways," *Proceedings of the IEEE 18th Digital Avionics Systems Conference*, IEEE Press, New York, 1999, pp. 4.C.3–1.

[4]Elliot, D., and Perry, B., "NASA Research for Instrument Approaches to Closely Spaced Parallel Runways," *Proceedings of the AIAA Guidance, Navigation, and Control Conference*, AIAA, Reston, VA, 2000.

[5]Carpenter, B., and Kuchar, J., "Probability-Based Collision Alerting Logic for Closely Spaced Parallel Approach," *Proceedings of the AIAA 35th Aerospace Sciences Meeting and Exhibit*, AIAA, Reston, VA, 1997.

[6]Houck, S., Barrows, A., Parkinson, B., Enge, P., and Powell, D., "Flight Testing WAAS for Use in Closely Spaced Parallel Approaches," *Proceedings of the ION-GPS 1999 Meeting*, Inst. of Navigation, Fairfax, VA, 1999, pp. 1787–1798.

[7]Pritchett, A. R., "Pilot Performance at Collision Avoidance During Closely Spaced Parallel Approaches," *Air Traffic Control Quarterly*, Vol. 7, No. 1, 1999, pp. 47–75.

[8]Winder, L. F., and Kuchar, J. K., "Generalized Philosophy of Alerting with Applications for Parallel Approach Collision Prevention," TR ICAT-2000-5, Massachusetts Inst. of Technology, Cambridge, MA, Aug. 2000.

[9]King, B. T., and Kuchar, J. K., "Evaluation of Collision Alerting System Requirements for Paired Approach," *Proceedings of the Digital Avionics Systems Conference* (DASC00), IEEE Press, New York, 2000, pp. 2.D.1–1.

[10]Landry, S., and Pritchett, A. R., "The Safe Zone for Paired Closely Spaced Parallel Approaches: Implications for Procedures and Automation," *Proceedings of the Digital Avionics Systems Conference* (DASC00), IEEE Press, New York, 2000, pp. 3.E.–1.

[11]Houck, S., and Powell, J. D., "A Parametric Sensitivity Study of Ultra Closely Spaced Parallel Approaches," *Proceedings of the Digital Avionics Systems Conference* (DASC00), IEEE Press, New York, 2000, pp. 2.D.4–1.

[12]Houck, S., and Powell, J. D., "Assessment of the Probability of a Midair Collision During an Ultra Closely Spaced Parallel Approach," *Proceedings of the AIAA Guidance, Navigation and Control Conference*, AIAA, Reston, VA, 2001.

[13]Waller, M. C., and Scanlon, C. H., "A Simulation Study of Instrument Meteorological Condition Approaches to Dual Parallel Runways Spaced 3400 and 2500 feet Apart Using Flight-Deck-Centered Technology," TR NASA/TM-1999-208743, March 1999.

[14]Koczo, S., "Coordinated Parallel Runway Approaches," TR NASA Contractor Rept. 201611, Rockwell International, Cedar Rapids, IA, Oct. 1996.

[15]Jennings, C., Charafeddine, M., Powell, J. D., and Taamallah, S., "Flight Demonstration of 3D Perspective Synthetic Vision and ADS(B) for Closely Spaced Parallel Approaches," *IEEE Proceedings of the 21st Digital Avionics Systems Conference*, IEEE Press, New York, 2002, pp. 11.C.1–1-11.

[16]Winder, L. F., and Kuchar, J. K., "Evaluation of Collision Avoidance Maneuvers for Parallel Approach," *Journal of Guidance, Control, and Dynamics*, Vol. 22, No. 6, 1999, pp. 801–807.

[17]Teo, R., and Tomlin, C. J., "Computing Provably Safe Aircraft to Aircraft Spacing for Closely Spaced Parallel Approaches," *Proceedings of the Digital Avionics Systems Conference* (DASC00), IEEE Press, New York, 2000, pp. 2.D.2–1.

[18]Teo, R., and Tomlin, C. J., "Provably Safe Evasive Maneuvers Against Blunders in Closely Spaced Parallel Approaches," *Proceedings of the AIAA Guidance, Navigation, and Control Conference*, AIAA, Reston, VA, 2001.

[19]"Minimum Aviation System Performance Standards for Automatic Dependent Surveillance-Broadcast (ADS-B)," Radio Technical Commission for Aeronautics, TR RTCA-186 DRAFT 4.0, Washington, DC, Feb. 1997.

[20]Prasad, U. R., Rajan, N., and Rao, N. J., "Planar Pursuit–Evasion with Variable Speeds, Part 1, Extremal Trajectory Maps," *Journal of Optimization Theory and Applications*, Vol. 33, No. 3, 1981, pp. 401–418.

[21]Isaacs, R., *Differential Games*, Krieger, Huntington, NY, 1975.

[22]Hansen, A. J., "Wide Area Augmentation System, Precision Approach Metrics: Accuracy, Integrity, Continuity and Availability," WADGPS Lab., Stanford Univ., Stanford, CA, Oct. 1999; also available at URL: http://waas.stanford.edu/metrics.html.

[23]Mukai, C., "Design and Analysis of Aircraft Dynamics Models for the ATC Simulation at NASA Ames Research Center," TR 91119-01, Seagull Technology, Inc., Campbell, CA, July 1991.

[24]Kuchar, J. K., "Methodology for Alerting-System Performance Evaluation," *Journal of Guidance, Control, and Dynamics*, Vol. 19, No. 2, 1996, pp. 438–444.